Crystallization, Dispersion Behavior and the Induced Properties Through Forming a Controllable Network in the Crosslinked Polyester-SiO_2 Nanocomposites

Wang Yu Guo, Ke Yang Chuan

State Key Laboratory of Heavy Oil Processing, Faculty of Chemistry and Chemical Engineering, China University of Petroleum, Beijing 102249, China

Received 23 April 2010; accepted 6 April 2011
DOI 10.1002/app.34643
Published online 19 August 2011 in Wiley Online Library (wileyonlinelibrary.com).

ABSTRACT: The poly(ethylene terephthalate) (PET) crosslinked copolymers (G-PET) with glycerol (GC) and their novel nanocomposite samples (GNPET) were reported and investigated. The nanoparticle dispersion behavior was creatively stabilized with the crosslinked network. Several interesting properties and phenomena including the abnormal crystallization behavior of GNPET samples were presented. Results of differential scanning calorimeter proved that the thermal and crystallization behavior of GNPET samples was effectively tuned with GC load. The obviously enhanced crystallization and nanoparticle homogenous dispersion behavior appeared at 2 wt % SiO_2 and 0.2 wt % GC load. Polarized optical microscopy (POM) results showed that the spherulite growth rate of the GNPET samples with 0.1 wt % GC load sharply decreased from 0.0562 to 0.0157 μm s^{-1} with 0.5 wt % GC load. As GC load increased, the spherulite size of GNPET samples decreased greatly so as to be much smaller than that of pure PET nanocomposites. Water absorbing experiments presented that the higher GC load created the lower water diffusion behavior but higher barrier against water, gas, and light. A model was proposed to state the network immobilization effect on the nanoparticle dispersion, and the restraining effect on PET chain mobility and crystal size growth which were related to the above properties. © 2011 Wiley Periodicals, Inc. J Appl Polym Sci 123: 1773–1783, 2012

Key words: poly(ethylene terephthalate); nanocomposites; crosslinking network; crystallization; dispersion

INTRODUCTION

Poly(ethylene terephthalate) (PET) thermoplastic polymer with excellent chemical and physical properties has applications in film, fibers, petroleum engineering, and barrier materials against water, gas, or even harmful light. Especially, in the field of petroleum engineering, solar cell, or fuel cell, PET polymer materials with enhanced crystallization and surface or barrier behavior are urgently required.

However, PET polymer has low crystallization rate, unstable surface properties or very low barrier behavior which affected its processing and functional applications.[1] Many efforts have been made on its crystallization kinetics and modifications.[2] Generally, incorporation of nanophase, such as SiO_2 nanoparticles or layered silicates, into PET improved its thermal, mechanical, and crystallization behaviors.[3–10] The nanoparticles could restrain the spherulite growth.[9,10] However, their agglomeration and unstable dispersion patterns usually affected the nanocomposite material processing behavior, gas permeability, and surface performance.[5–8]

In the previously established dispersion methods, the intercalation of the layered silicates and particle surface treating were popular. In the intercalation polymerization process,[5–13] the nanoparticles *in situ* formed and dispersed well in the polymer matrix to obviously improve the crystallization behavior.[11–13] When the nanoparticles dispersed in PET, they acted as the heterogeneous nucleation centers to accelerate the crystallization process.[14] These dispersion methods still need improving to avoid the reconnections or agglomerations of the dispersed particles. That is, the nanoparticle dispersion patterns need stabilizing. Recently, the nanoparticle crosslinking with PET side chain in a solid polymerization was reported to immobilize their dispersion patterns in PET matrix.[15] For the SiO_2 nanoparticles, the optimized load improved the dispersion stability in PET.[16] Besides, the pure PET, properly crosslinking copolymers, effectively tune its crystallization behavior.[17] Thus, if this PET crosslinking structure was combined with the nanoparticles to establish a novel stabilized particle dispersion, PET crystallization behavior and properties were expected to enhance.

Correspondence to: K. Y. Chuan (key@cup.edu.cn).
Contract grant sponsor: National Science Foundation; contract grant numbers: 20776157, 21076229.
Contract grant sponsor: National Key Special Project; contract grant numbers: 2008ZX05022-04, 2008ZX 05009-05.

In this article, PET crosslinking copolymers with glycerol (GC) monomer and their nanocomposites with SiO_2 nanoparticles were reported. The controllable networks for the nanoparticle dispersion were created so that the PET molecular chain polarity was enhanced and chain mobility reduced.[18,19] These SiO_2 nanoparticles were expected to disperse homogeneously and to be immobilized in the network chains which were suitable for forward stably processing.[20] This creative design provided the high-performance PET nanocomposite materials with enhanced crystallization and stable surface behavior which would find their applications to functional materials for petroleum engineering.

EXPERIMENTAL

Materials and experiment apparatus

SiO_2 nanoparticles with an average of 30 $\sim$ 50 nm size (average 40 nm) were obtained from Jiangsu Haihe Nanomaterial Technology. γ-Methacryloxypropyl trimethoxy silane (MPS) reagent, analytical grade (AR), Beijing Chemical Reagent has a double bond in its molecular structure. This molecular modified SiO_2 nanoparticles[13,14,16] were made in our laboratory. Monodisperse SiO_2 nanoparticles prepared in our laboratory through observing the process in the literature[21–23] acted as standard only for characterizing the multiscale SiO_2 nanoparticles. Pure *p*-terephthalate (PTA) a monomer of Industry Grade (IG) was obtained from LiaoYang Petrochemical Institute; ethylene glycol (EG) a monomer (IG) was obtained from Beijing Hongxing Chemical; GC a crosslinker monomer analytical grade was obtained from Beijing Modern Eastern Fine Chemical Product; Other reagents, market sales analytical grade. Supersonic machine, KQ3200DE, KunShan Supersonic Device; Autoclave of super high-vacuum system for esterification and polymerizations, 12 L, was designed in our laboratory.

Polymerization and Preparations

Preparing GNPET samples

Generally, preparing the polyester oligomer is the necessary step for further preparing the high molecular mass of final polyester polymers. Thus, preparing the GNPET must include the two steps as below.

Preparing BHET from esterification reaction. In this process, all monomers and additives are mixed together to proceed the esterification reaction. Here, the MPS-modified[13,14,16] SiO_2 nanoparticles were dispersed in EG to form the suspensions to which different GC monomers were added. Then, at the molar ratio of 1.4 : 1 for EG to PTA, the temperature rose and the esterification reaction occurred at 230 $\sim$ 250°C and at the pressure of 0.25 Mpa. This heating temperature was kept so as to maintain the top-condensing column temperature below 50°C. The temperature rose to 260°C while the pressure did not rise. Then, the hydroxyethyl methacrylate oligomer (BHET) was prepared, and this oligomer went through further polymerization to prepare the high molecular mass of polyesters.

Polymerization reaction. The prepared BHET oligomers were made into powders. Then, to 3.15 kg of BHET powders in the autoclave reactor, the 500 ppm Sb_2O_3 powder catalysts relative to BHET and 200 mL EG monomers were added. The reaction mixtures were heated to melt and stirred while the temperature reached 280°C. The initial rough vacuum pressure was gradually tuned below 200 Pa but the high vacuum degree for BHET polymerization could reach below 1 Pa for about 1 $\sim$ 3 h. When the speed of the stirring impeller reduced to 20 r min^{-1} and basically did not change for another 2 $\sim$ 3 h, the vacuum system was shut down while the nitrogen gas was purged inside the autoclave reactor so as to extrude the melt. The GNPET pellets were obtained from the attached cutter. The physical properties of the GNPET samples of different SiO_2 nanoparticles and GC load were shown in Table I.

Preparing the compressed composite films

The PET powders were screened with a sieve of 100 meshes, and then sealed in a copper mould under a specific pressure, and sandwiched between two 0.50-mm-thick aluminum films. They were pressed at 275°C and 10 $\sim$ 16 MPa for 5 min on a tablet machine of 769YP-60E, TianJin Ke Qi High-Tech, China. Then, they were rapidly quenched in the ice–water mixture media to obtain the amorphous PET and GNPET nanocomposite film samples with 0.5 mm thickness.

Characterizations and measurements

Thermal and crystallization measurements

Thermal and crystallization behaviors were performed with the NETZSCH DSC 204 F1 Phoenix differential scanning calorimeter (DSC). The sample thermal history was removed by melting them at 300°C for 5 $\sim$ 6 min, and the wholly amorphous samples were obtained by quenching the melt into liquid nitrogen. Then, the amorphous samples were heated from 25 to 300°C at a rate of 10°C min^{-1} to obtain DSC curves and thermal parameters.

Observation of particle dispersion and nucleation morphology

The amorphous film samples of 0.5 mm thickness were used here. Their plain and fractured surface was covered with gold film under a spray machine attached on S-4200 type Scanning Electronic

TABLE I
The Composition and Physical Properties of PET and GNPET Samples

Sample No	Glycerol load (wt %)	Nano-SiO_2 load (wt %)	Intrinsic viscosity (dl/g)	Transmittance[a] (%)
PET	0.0	0.0	0.680	84.06
GNPET-1	0.1	2.0	0.668	65.57
GNPET-2	0.2	2.0	0.691	72.24
GNPET-3	0.3	2.0	0.662	66.48
GNPET-5	0.5	2.0	0.643	67.51

[a] Optional transmittance: $T_t = (T_2/T_1) \times 100\%$ (The standard error of data of Intrinsic viscosity is ±0.2%; The standard error of data of transmittance is ±1.5%).

Microscopy (SEM), Japan. For this physical vapor depositing (PVD) process, PVD time of spraying gold was set to be 15 ~ 90 s, which depends. PVD-coating films were observed on SEM at 20 kV.

The morphology of the spherulite growth was taken for the annealed film samples. The mixtures of PET and GNPET powders were dissolved in trifluoroacetic acid and cast on the glass subtract, which was similar to a reported process.[22,24] The crystallization behavior was observed directly on the Olympus BH-2 polarized optical microscopy (POM) attached with a Linkam LTS 350 hot stage. The samples were melted in the platform at 300°C, lasted for 5 min to remove thermal history, and then quickly cooled to 220°C to *in situ* crystallize. The crystallite morphology pictures were automatically taken during *in situ* observation at 2-s interval which was set before the experiments. In this way, a set of the spherulite morphology pictures in the different crystallization periods were recorded.

The measurements of the water absorption and wettability

The absorption water experiment of the films followed the process in the literature.[9,10] After the film samples were placed into an oven and dried for 24 h at 50°C under reduced pressure, the films were quickly shifted into a desiccator and cooled to the room temperature. They were weighed on an attached analytical balance giving the initial weight of the films, and then the films were immersed in water at 25°C in a thermostate jar that was held in a water bath with its temperature controlled throughout the experiment. At designed time interval, weighing the film samples gave the weight at time t. The absorption water weight (Δm_t) of the films at time t was ($\Delta m_t = m_t - m_0$). The water absorption weight percentage (m_p) of the films at time t was.

$$m_p = [(m_t - m_0)/m_0] \times 100\% \quad (1)$$

According to Fick's first and second law,[25–28] m_t is a function of $t^{1/2}$. The plot of m_t against $t^{1/2}$ gave Fickian curves. On Fickian curves, the initial section was nearly linear. While, the polyester film sample during water absorbing process has a balance between absorbing and desorbing behaviors. The diffusion coefficient D was obtained from the slope of the initial section calculated with formulae (2).[25,28]

$$D = \frac{\pi}{16}\left(\frac{Sl}{C_\infty}\right)^2 \quad (2)$$

where l is the thickness of one film; C_∞ is the absorbing weight or mass percentage for each equilibrium absorbing process. S is the solubility coefficient from the slope of initial Fickian curve. The permeability coefficient P was defined as follows,

$$P = \mathrm{S} \cdot D \quad (3)$$

Such formulae also apply to describe the gas permeation process.

The wettability or contact angle, θ, was measured on a static drop contact angle/interface tension meter, JC2000A (Shanghai Zhongchen Digital Technical Equipment, China), with a θ error ± 2°. A 10-μL sampling device was used to transfer distilled water (pH = 7.0), and the water was dripped off from the location of 10 cm above the film sample table, and then the water was dropped off. After 30 s, θ value of the film sample was measured. The average θ data of five different points were taken as the final contact angle.

Measurements of the oxygen permeation

The permeation experiment observed the process in the test standard of GB/T 1038-2000 (GB/T1038-2000, Eqv. ISO2556-1974, see http://www.csres.-com/ upload /qy/168/GB-T%201038-2000.pdf).

The quantity (Q_g) for one gas going through a film has their formulae as below.

$$Q_g = \frac{\Delta p}{\Delta t} \times \frac{V}{A} \times \frac{T_0}{p_0 T} \times \frac{24}{p_1 - p_2} \quad (4)$$

where Q_g has unit of $cm^3\ m^{-2}$ d Pa; $\Delta p/\Delta t$ is an average pressure variation at low pressure chamber and steady permeation state, Pa h^{-1}; V is the volume of low-pressure chamber, cm^3; A is an effective test area for one film sample, m^2; T_0 and p_0 are the temperature of 273.15 K and pressure of 1.0133×10^5 Pa at the standard state, respectively; T is the test temperature, K; ($p_1 - p_2$) is the pressure difference at both sides of one film, Pa. Then the gas permeability coefficient (P_g) was calculated as follows,

$$P_g = \frac{\Delta p}{\Delta t} \times \frac{V}{A} \times \frac{T_0}{p_0 T} \times \frac{l}{p_1 - p_2} \quad (5)$$

where P_g has unit of cm^3 cm $(cm^2\ s\ Pa)^{-1}$; $\Delta p/\Delta t$ is the same as that in formulae (4), Pa/s; l is sample thickness, cm.

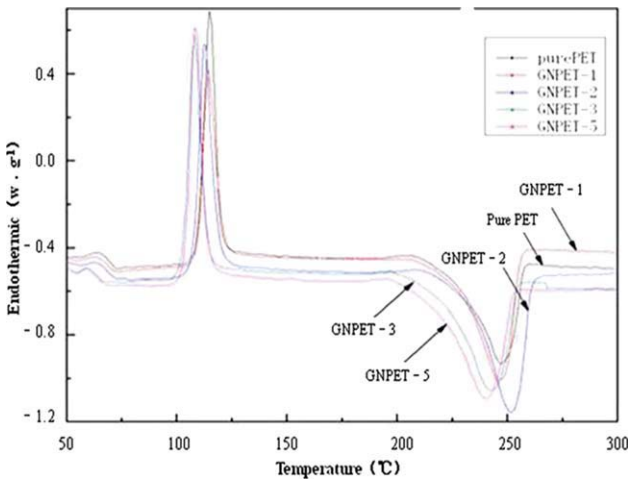

Figure 1 DSC endothermic curves of PET sample and GNPET composite with different crosslinker glycerol. [Color figure can be viewed in the online issue, which is available at wileyonlinelibrary.com.]

The optical measurements

The optical parameters of the transmittance (T_t) of the amorphous samples were measured on a WGW optoelectronic meter with an error ±2%, Shanghai Pudong Physical Optical Apparatus Factory Shanghai, China. Transmittance was defined as the percent ratio of the luminous flux of transmitted light to that of the incident light. The transmittance was given in the following equation:

$$T_t = (T_2/T_1) \times 100\% \quad (6)$$

where T_t is the transmittance, T_2 is the luminous flux of the transmitted light, and T_1 is the luminous flux of the incident light. Here, T_1 is set as 100.

The measurement process was performed according to the standard GB2410-80 (recently update GB/T 2410-2008, Eqv. ASTM D1003-61 (1997), see http://d.namipan.com/d/de24c7678c337e7765 a2bbe 7b08 cd 67a50cdb99959080600). Then, the results of the amorphous samples were compared with the isothermal-crystallized samples which were held at 130°C for 4 h in vacuum oven.

RESULTS AND DISCUSSION

The sample composition and properties

The sample composition and their basic properties were shown in Table I. It was seen in Table I that the properties of both viscosity and optical transmittance of PET copolymer samples were quiet sensitive to the GC load. Thus, GNPET sample was optimized at 2.0 wt % SiO_2 nanoparticle and 0.2 wt % GC load in which the optical transmittance kept the highest level.

Thermal and crystallization behavior

DSC patterns for melting and crystallization properties of PET nanocomposite samples were shown in Figure 1. T_{cc} represents the temperature in which the sample crystallizes from the amorphous or cold state. The lower T_{cc} represents the easier crystallization and nucleation growth process. ΔT_{cc} is another parameter to characterize the relative crystal nucleation rate of one sample. Usually, $\Delta T_{cc} = T_{cc} - T_g$, that is, the lower ΔT_{cc} created the rapid nucleation process.

Figure 1 showed that, at the fixed SiO_2 nanoparticle load, T_g of GNPET samples was quiet sensitively tuned with the crosslinker GC load. When GC load surpassed 0.2 wt %, T_g varied slightly compared with pure PET. Very high GC load might create the extra heterogeneous crosslinking network when SiO_2 nanoparticles were introduced to PET. Both the nanoparticles and GC load were the factors on forming the PET networks. The results in Figure 1 were summarized in Table II. There, at 0.3 and 0.5 wt % GC load, T_g of GNPET samples reduced to 67.5 and 67.3°C, respectively, compared to 69.4°C of pure PET. T_g of GNPET-5 sample was 2.1°C lower than that of the pure PET. Similarly, T_g of pure PET-SiO_2 nanocomposite sample reduced and was lower than that of pure PET which were compared to these GNPET samples in Table II. Similar results to these were seen in the works of Wu, Wang, and Yuan.[28,30,31] For such phenomenon of T_g slight

TABLE II
The Thermal and Crystallization Behavior of GNPET Samples

Samples	SiO_2 load (wt %)	Glycerol load (wt %)	T_g (°C)	T_{cc} (°C)	T_m (°C)	ΔT_{cc} (°C)	ΔH_m (J g^{-1})	X_t (%)
PET	–	–	69.4	115.1	247.3	45.7	59.45	50.55
GNPET-1	2.0	0.1	68.2	114.3	245.9	46.1	73.36	62.38
GNPET-2	2.0	0.2	68.5	112.7	251.7	44.2	76.54	65.08
GNPET-3	2.0	0.3	67.5	113.5	244.7	46	61.42	52.22
GNPET-5	2.0	0.5	67.3	116.2	243.1	48.9	57.92	49.25

Fusion enthalpy according to DSC measurement, samples heated from 25 to 300°C min^{-1} with a heating rate of 10°C min^{-1}. Relative crystallinity calculated from the measured fusion enthalpy against the fusion enthalpy (117.6 J g^{-1}) of the fully crystallized PET homopolymer.[29] (The standard error of data of T_g is ±2.0%.)

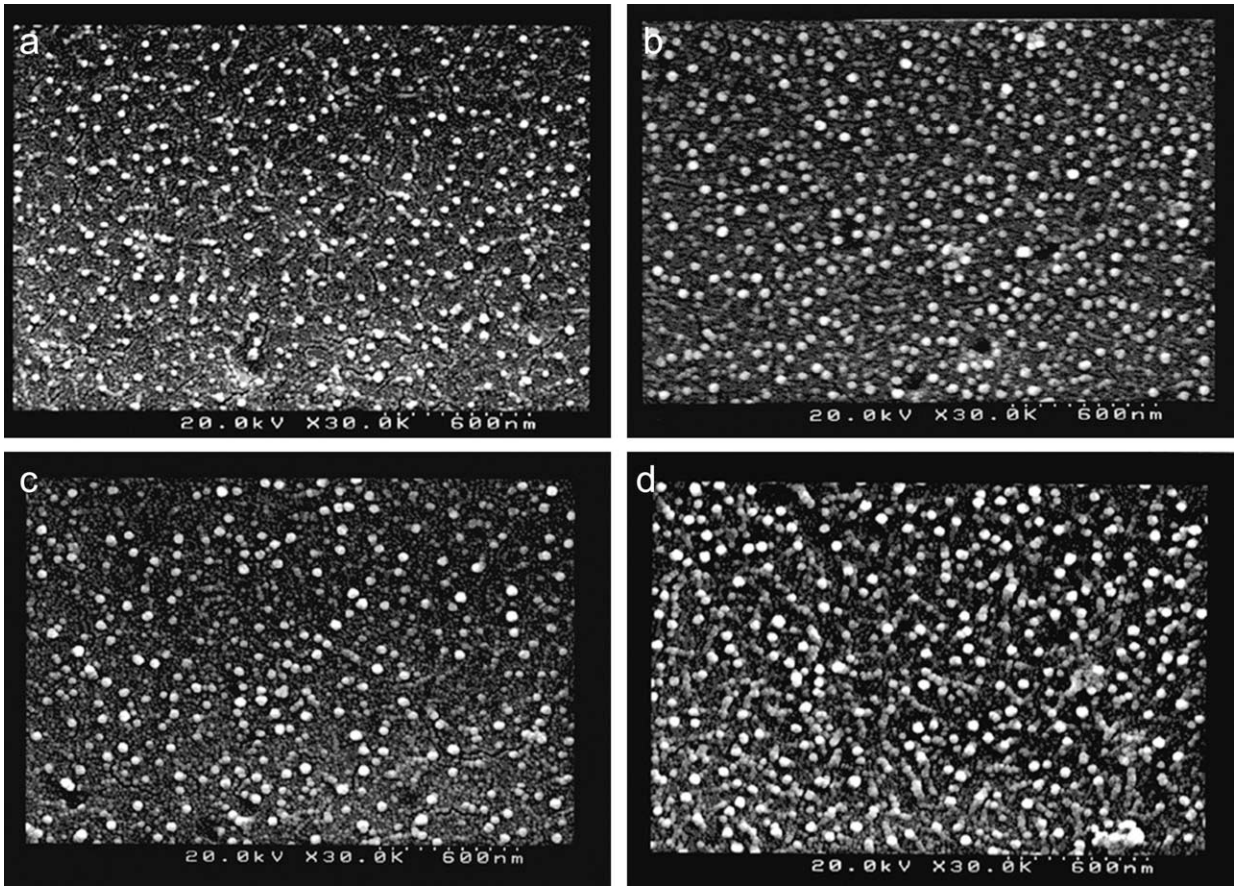

Figure 2 SEM images of amorphous GNPET nanocomposite samples with crosslinker glycerol load (sample prepared through a process of melting and quenching in the ice water media; (a) GNPET-1, 2 wt % SiO_2 and 0.1 wt % glycerol). (b) GNPET-2, 2 wt % SiO_2 and 0.2 wt % glycerol; (c) GNPET-3, 2 wt % SiO2 and 0.3 wt % glycerol; (d) GNPET-5, 2 wt % SiO2 and 0.5 wt % glycerol.

reduction, it was thought that introducing nanoparticles to PET increased its molecular chain activity so as to increase chain movement which might affected $T_{g.}$ of final GNPET sample. Thus, only introduction of the crosslinking comonomer GC to PET did not obviously increase its T_g.

In Table II, as the crosslinker GC increased, both the cold crystallization peak T_{cc} and ΔT_{cc} of GNPET samples increased except GNPET-2, indicating that it was difficult for GNPET samples to nucleate at the lower temperature than that of PET.

The phenomenon that the GNPET-2 sample showed the lowest values of T_{cc} and ΔT_{cc}, but the highest crystallization degree or rate is thought to be resulted from the optimum loads. That is, at 2.0 wt % SiO_2 nanoparticle load and 0.2 wt % GC load, both the GC crosslinking network density and nanoparticle dispersion behavior might reach the most optimized or ideal state. Obviously, this critical load point is just what we were looking for from the experiments.

For other samples in Table II, the excessively more hydroxyl groups might restrain the more PET molecular chain mobility so that their thermal behavior could keep stable but their crystallization behavior was affected. Compared with PET, the SiO_2 nanoparticles increased the heterogeneous nucleation effect or nucleation density on the GNPET samples. The formation of proper crosslinked PET molecular chain network with GC might balance PET crystallization behavior. In this way, PET polymer with crosslinking network structure might crystallize homogeneously.

DISPERSION AND CRYSTALLIZATION BEHAVIOR

Nanoparticle dispersion behavior in the crosslinking network

SEM morphology of the nanoparticle dispersion was shown in Figure 2. It was seen that, as the crosslinker GC load increased, the network of the active hydroxyl groups with the SiO_2 nanoparticles formed different morphology. In Figure 2, 2 wt % SiO_2 nanoparticle load created the satisfied and stable

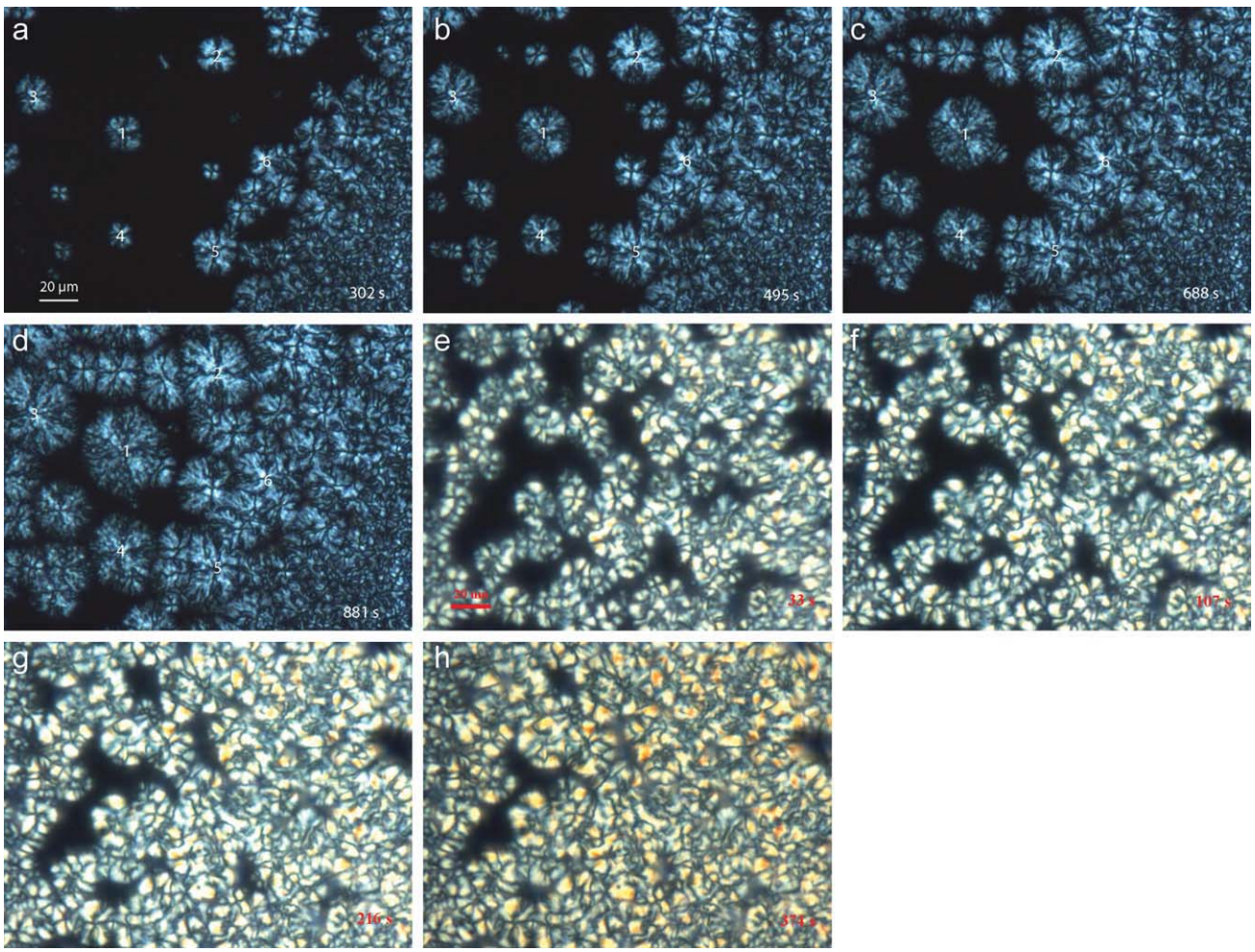

Figure 3 POM spherulite morphology of the GNPET-2 samples at different crystallization time during the crystal growth at 220°C from the melt: (a) 302 s, (b) 495 s, (c) 688 s, and (d) 881 s; and POM spherulite morphology of the GNPET-5 samples at different crystallization time during the crystal growth at 220°C from the melt: (e) 33 s, (f) 107 s, (g) 216 s, and (h) 374 s. [Color figure can be viewed in the online issue, which is available at wileyonlinelibrary.com.]

dispersion behavior. The previously preparing the GNPET samples and their characterizations have shown that the crosslinking degree of PET molecular chain greatly increased as GC load increased. While, at the relatively low crosslinker GC load, the crosslinking degree or network density of PET molecular chain was relatively low, thus, parts of the SiO_2 particles could be embedded in the network of PET chains and enter the free volume of PET matrix seen in Figure 2(a). So, these dispersed SiO_2 nanoparticles seem to be smaller than their original size of 30 $\sim$ 50 nm (average size 40 nm).

In Figure 2(b,c), as GC load further increased, PET molecular chains became more and more active. Some SiO_2 nanoparticles took scattered patterns which were not totally embedded in PET chains or just floated on the surface of the crosslinking networks. Figure 2(d) showed, as the crosslinker load increased, the chain network might be heavily compacted, most of the SiO_2 nanoparticles just floated on the relatively stable crosslinked networks while might not enter into the free volume of the PET matrix. So, the average size of SiO_2 nanoparticles in GNPET-5 seems to be bigger than that in GNPET-1 sample.

Furthermore, one hundreds of SiO_2 nanoparticles were selected randomly from SEM graph of Figure 2(a–d) to calculate the average particle size. The obtained average size of the SiO_2 nanoparticles in GNPET-1, GNPET-2, GNPET-3, and GNPET-5 samples was 31.04, 33.74, 36.45, and 38.24 nm, respectively. The SiO_2 nanoparticle size before and after the polymerization should keep constant.

However, these SiO_2 nanoparticles in PET matrix became larger and larger in size as the crosslinker GC load increased. In the optimized case (say, 0.2 wt % GC, 2 wt % SiO_2 load), the particles took a relatively stable dispersion pattern in which the average size of SiO_2 nanoparticle was 33 nm comparing to the original 30 $\sim$ 50 nm (40 nm in average). This phenomenon was thought to be resulted from that the formed networks had their chain crosslinking

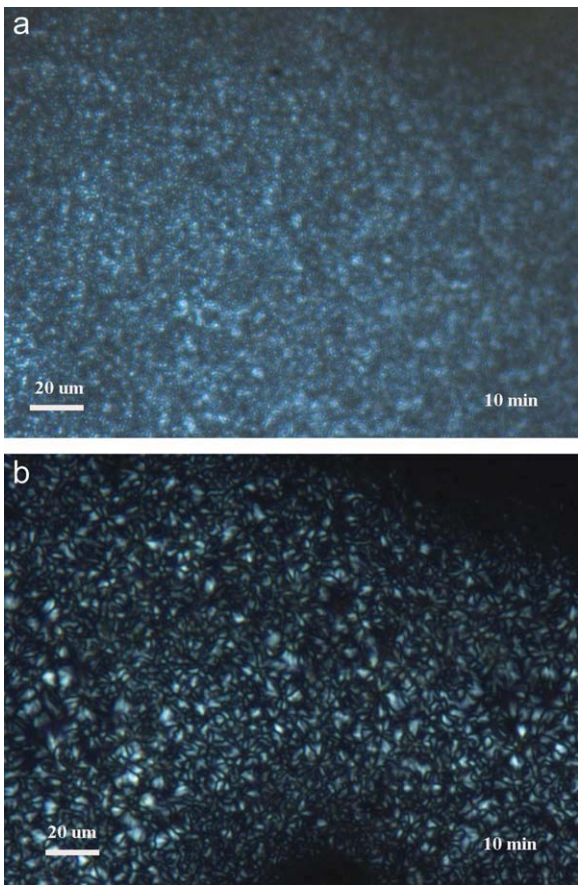

Figure 4 (a) POM spherulite morphology of (a) the pure PET sample at 10 min crystal growing at 220°C from the melt and (b) the GNPET-1 sample at 10 min crystal growing at 220°C from the melt. [Color figure can be viewed in the online issue, which is available at wileyonlinelibrary.com.]

density to be tuned with GC load. Thus, the more nanoparticles were excluded from the PET network at higher GC load. So, the appropriate network density was required to provide a way for the SiO_2 nanoparticles to stably disperse in PET matrix.

The spherulitic growth behavior in the crosslinking network

The crosslinking network has direct effect on PET crystallization behavior. The crystallizing morphology of the GNPET-2 and GNPET-5 samples was illustrated in Figure 3. As for these GNPET samples, during tracing measurements of their spherulite radius of some selected crystals at different crystallization time, the spherulite growth rate was *in situ* recorded. The crystallite morphology was *in situ* taken automatically during the observation process at a 2-s interval set before the measuring experiments.

In this way, the obtained were a set of the spherulite morphology pictures in their different crystallized periods. The spherulite growth rate for the GNPET-1, GNPET-2, GNPET-3, and GNPET-5 samples in a specially designed time range were obtained (see later part). But some samples were not easy to record the perfect spherical morphology because of the different nucleation density (Fig. 4).

In Figure 4, some spherulite morphology approached the crystallization end. During observing the spherulite morphology of pure PET and GNPET samples, it took many times of try-and-error to record the satisfied spherulite morphology. Their grown crystals either scarcely distributed (PET) or collided heavily to form small broken spherulite morphology (GNPET-1). So, the too low crosslinker GC load only produced the low effective network for the spherulite growth. During the crystallization process, tracing the growth rate of the spherulite size of these samples was plotted against the crystallization time shown in Figure 5.

From the curves and their slopes shown in Figure 5, for these four samples of the same 2 wt % SiO_2 particle load the obtained spherulite growth rate was as such, 0.0562 μm s^{-1} for GNPET-1 (0.1 wt % GC load), 0.0242 μm s^{-1} for GNPET-2 (0.2 wt % GC load), 0.0154 μm s^{-1} for GNPET-3 (0.3 wt % GC load), and 0.0157 μm s^{-1} for GNPET-5 (0.5 wt % GC load), respectively. These growth rates have an error ±0.0002 μm s^{-1}. The spherulite growth rate showed an obvious downward trend or four times decrease as GC load increased from 0.1 to 0.5 wt %. During the experimental times, the average spherulite size for these samples was as such, GNPET-1: 33.59 μm, GNPET-2: 25.92 μm, GNPET-3: 19.00 μm, and GNPET-5: 18.83 μm. These spherulite sizes have an error ±0.20 μm.

These results strongly proved that, the molecular crosslinking network effectively affected the spherulite growth rate and size. The higher GC load produced the lower spherulite growth rate and size. Comparatively, in the GNPET samples, the

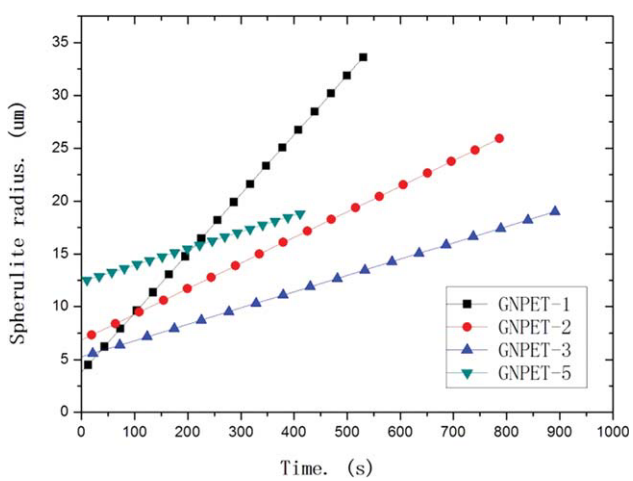

Figure 5 The plot of the spherulite radius growth versus its growing time of the GNPET samples. [Color figure can be viewed in the online issue, which is available at wileyonlinelibrary.com.]

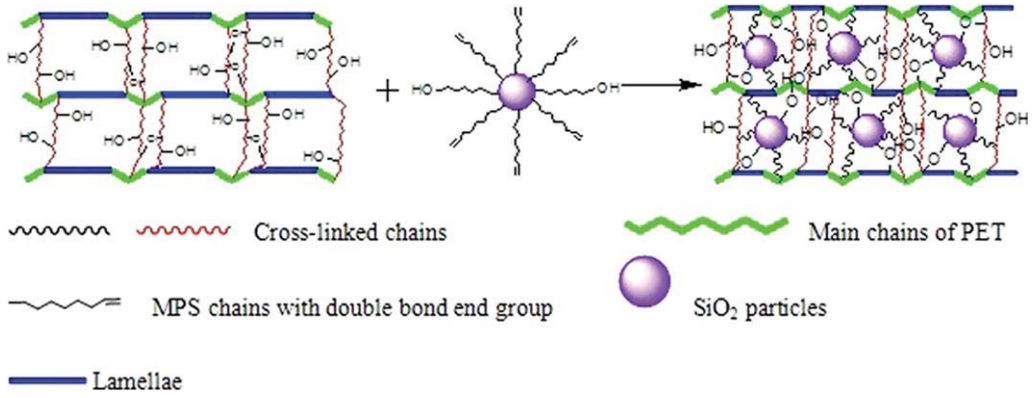

Figure 6 A model showing the treated nanoparticle dispersing in PET matrix and their affecting its lamellae morphology and amorphous connecting chains. [Color figure can be viewed in the online issue, which is available at wileyonlinelibrary.com.]

spherulite size was reduced more obviously and effectively than that in the pure PET or noncrosslinked PET with SiO_2 nanocomposites.

Besides, comparing T_{cc} results in Table II, DSC gave the average results of GNPET samples which were not sensitive to the minor increase of GC load. While, such results were satisfactorily consistent with these from the measured spherulite growth in the GNPET samples. Obviously, the spherulite growth rate for GNPET samples was an important or sensitive reference to evaluate the crystallization behavior.

Based on the above crystallization behavior induced with both the heterogeneous nucleating effect of SiO_2 nanoparticles and the crosslinking networks, a brief model was suggested to show the process of the nanoparticles diffusing in PET matrix and affecting the crystal size of the lamellae (see Fig. 6).

The property variation of these GNPET samples was thought to be resulted from the effect of both the network reducing the chain mobility and the nanoparticle nucleation. The nanoparticles absorbed the amorphous chains varied PET lamellae morphology and obviously reduced its spherulite size. This might enhance the surface, barrier against gas or thermal stability performance of PET polymers.

THE BARRIER BEHAVIOR OF THE NANOCOMPOSITE SAMPLES

The water vapor absorbing behavior

The nanoparticle dispersion through the crosslinking network created the diverse properties of the GNPET samples. The water vapor absorbing behavior for GNPET samples was shown in Figure 7. In the case of Fickian absorbing model,[26–28] the absorption curves had shown an initial stage followed by a plateau which indicated an equilibrium state. The curves showed a zig-zag pattern reflecting that the water molecules penetrated or jumped from one position to another, permeated toward the depth of the films. From the linear section, the mean diffusion coefficient D for each vapor activity was obtained, and S was calculated from the curve slope at initial absorbing linear stage (left region of dashed line in Fig. 7).

Based on the eq. (5), the diffusion coefficient D and permeability coefficient P were calculated from Figure 7, and they were summarized in Table III. It was seen that the crosslinking samples have their permeability P of 11.6 $\sim$ 61.0% much lower than that of the pure PET. These crosslinking samples enhanced greatly the barrier properties against water. The reasons for such phenomena are addressed here. Under the moisture conditions, the

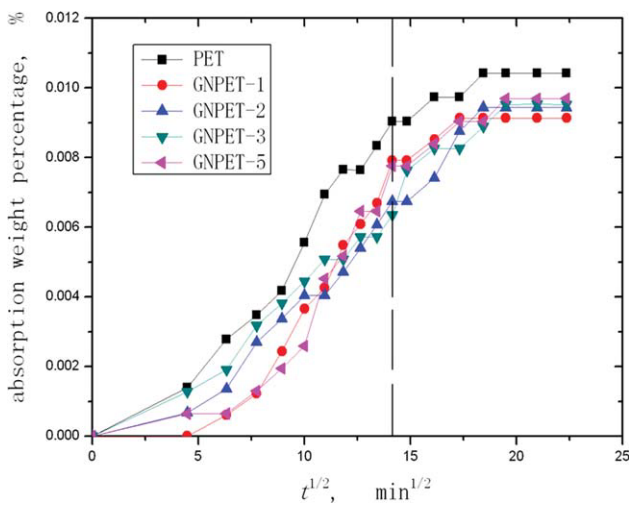

Figure 7 Fickian curves of the absorption water behavior with the crosslinker glycerol load for the amorphous GNPET samples (PET, 0 wt % SiO_2 and 0 wt % glycerol; GNPET-1, 2 wt % SiO_2 and 0.1 wt % glycerol; GNPET-2, 2 wt % SiO_2 and 0.2 wt % glycerol; GNPET-3, 2wt % SiO_2 and 0.3 wt % glycerol; GNPET-5, 2 wt % SiO_2 and 0.5 wt % glycerol). [Color figure can be viewed in the online issue, which is available at wileyonlinelibrary.com.]

TABLE III
The Film Surface Behavior Based on the Water Absorbing Experiments

Samples	GE load (wt %)	S ($\times 10^{-4}$ $min^{1/2}$)	C_∞ (%)	D ($\times 10^{-12}$ m^2 s^{-1})	P ($\times 10^{-14}$ m^2 $s^{-1/2}$)	Θ (°)
PET	0.0	6.83	1.042	3.515	1.860	72.0
GNPET-1	0.1	6.05	0.924	3.508	1.644	101.0
GNPET-2	0.2	5.04	0.943	2.337	0.912	99.1
GNPET-3	0.3	4.70	0.952	1.994	0.726	94.7
GNPET-5	0.5	5.82	0.969	2.952	1.331	78.0

Notes: S, the solubility coefficient; C_∞, the equilibrium absorption quantity; D, diffusion coefficient; P, permeability coefficient; Θ, contact angle (The standard error of data of Θ° is ±2.0%).

crosslinking network could reduce both PET molecular chain expansion, relaxation, and solubility behavior (see S in Table III). The reasons were as such, the more hydroxyl end groups in GNPET molecular chains created their higher chain polarizations so as to immobilize the more water molecule movements than did these in the pure PET.

The surface behavior of the GNPET samples

The water drop morphology in the contact angle (θ) experiments was shown in Figure 8. With a drop of water on the five different locations of the film surface, the average θ value was obtained and summarized in Table III.

Pure PET film with hydroxyl groups has wetting angle of 72.0°, showing hydrophilic behavior or a certain absorption capacity. As seen in Figure 8, when different crosslinker GC and SiO_2 particles were loaded, the film contact angle was greater than 90.0°, indicating their hydrophobic or dewetting behavior. This phenomenon was thought to be resulted from both the partially hydrophobic surface of treated SiO_2 particles and the possible surface roughness formed from both the crosslinking network and dispersed SiO_2 nanoparticles (see a model in Fig. 6). The surface roughness has a great effect on the hydrophobic behavior.[32,33]

As the crosslinker GC load increased, the film hydrophobicity decreased. This was because the more hydroxyl groups of GC introduced to PET chains could produce the higher hydrophilic behavior.

Optical barrier behavior

The barrier behavior against the visible light for the amorphous and annealing samples (0.5 mm thick) was investigated and shown in Figure 9. The optical transmission of the amorphous GNPET samples or their transparency was much higher than that of the crystallized one. The maximum optical transmission of this amorphous GNPET film approached 90%. As GC load increased, the light transmittance of GNPET

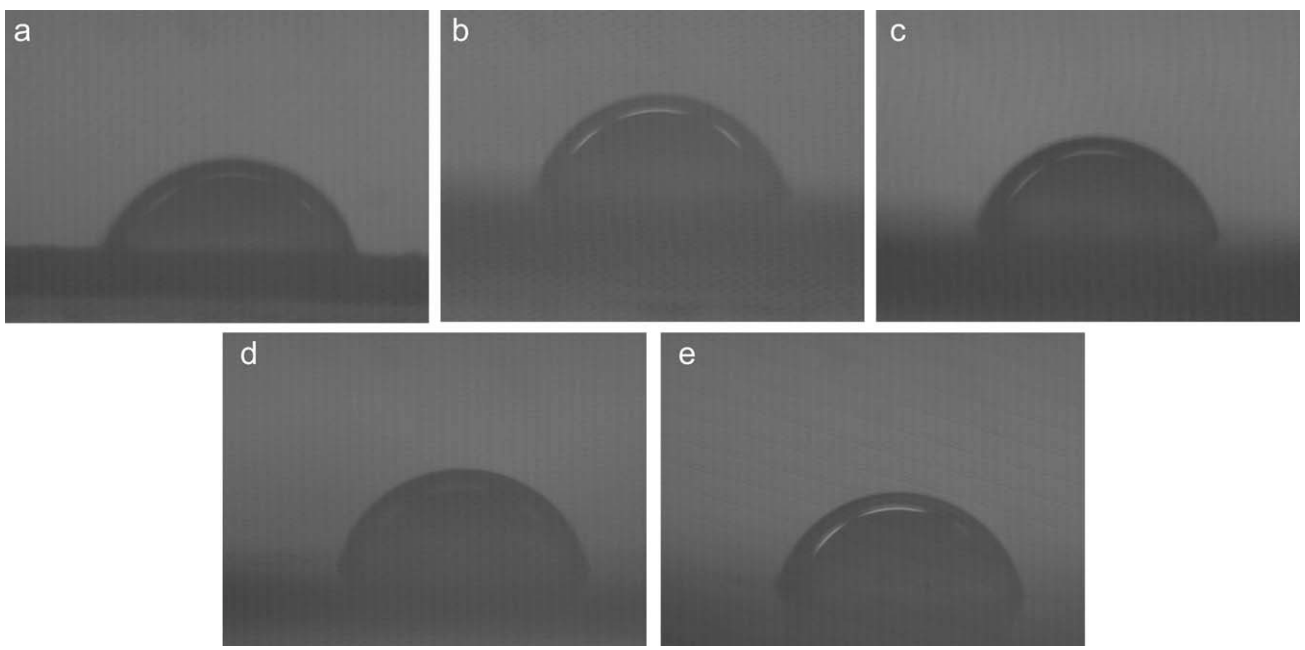

Figure 8 The effect of the crosslinker glycerol load in the sample on its contact angle (a) PET, (b) GNPET-1, (c) GNPET-2, (d) GNPET-3, and (e) GNPET-5.

sample further decreased. This clearly stated that the SiO_2 nanoparticles in the GNPET samples created a homogeneous dispersion pattern, and an obvious effect on the crystallization and nucleation behavior of PET so as to form the induced sized crystals. The light was relatively hard to transmit through the crystalline area compared to amorphous area as the SiO_2 nanoparticles could induce the heterogeneous nucleation to form the different sized crystals. These crystals formed in the crystallized GNPET sample together with SiO_2 nanoparticles and the crosslinked network produced barrier against the light transmittance.

Gas barrier properties

The O_2 gas permeation behavior for GNPET-2 and pure PET samples was briefly investigated. Based on eqs. (5) and (6) and testing standard GB/T1038-2000 (GB/T 1038-2000, Eqv.ISO2556-1974, http://www.csres.com/upload/qy/168/GB-T%201038-2000.pdf), the obtained results were shown in Table IV. The gas permeability of the GNPET film sample was much lower than that of the pure PET. GNPET-2 sample reduced 40.7% permeability quantity while its permeability coefficients reduced 29.6%. That is, the crosslinker GC and SiO_2 nanoparticles enhanced the gas barrier behavior. The reasons might be briefly explained as such the SiO_2 nanoparticles could induce to form more fine crystals and crystallized area in the crosslinked GNPET samples than these in the pure PET or pure PET-SiO_2 nanocomposite samples. While further details of such barrier phenomenon in the GNPET films will be shown elsewhere.

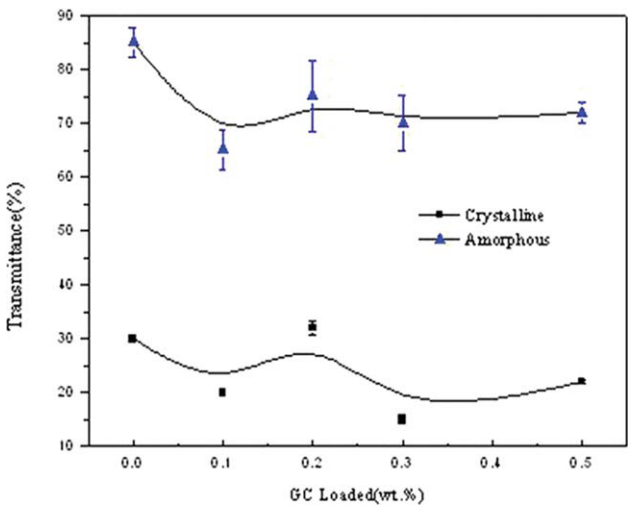

Figure 9 The light transmittance of the amorphous/crystalline samples with different glycerol load (amorphous samples crystallized at 130°C for 4 h). [Color figure can be viewed in the online issue, which is available at wileyonlinelibrary.com.]

TABLE IV
The O_2 Gas Permeation Behavior for the GNPET-2 and Pure PET Samples

Samples	O_2 quantity ($cm^3\ m^{-2}\ d^{-1}\ Pa^{-1}$)	O_2 permeation coefficient ($\times 10^{-15}\ cm^3\ cm\ cm^{-2}\ s^{-1}\ Pa^{-1}$)
PET	9.81	10.05
GNPET-2	5.82	7.08

The standard error of data of O_2 permeation coefficient is ±2.0%.

CONCLUSIONS

1. In PET polymer chain crosslinked networks with GC, SiO_2 nanoparticle dispersion behavior was obviously improved. At the optimized 2 wt % SiO_2 load, the stable dispersion patterns formed through the network immobilizing these particles.
2. The crosslinker GC was slew down PET isothermal crystallization rate, and obviously reduced its spherulite size as its molecular chain mobility was restrained. SiO_2 nanoparticles in the crosslinked networks activated PET molecular chains and created homogenously growing PET crystals through their nucleation effects.
3. As both the crosslinker GC and nanoparticle load were optimized, the PET water equilibrium absorption and hydrophobic properties were improved. Its barrier behavior against water, gas, and visible light was obviously enhanced as the GNPET sample crystallization behavior was induced with both crosslinking network and nanoparticles.

References

1. Scheirs, J.; Long, T., Eds. Modern Polyesters; Wiley: Chichester, New York, 2003.
2. Lu, X. F.; Hay, J. N. Polymer 2001, 42, 9423.
3. Pinnavaia, T. J.; Beall, G. W. Eds. Polymer-Clay Nanocomposites; Wiley: New York, 2000.
4. Zoppi, R. A.; Nunes, S. P.; das Neves, S. Polymer 2000, 41, 5461.
5. Hu, Y. S.; Hiltner, A.; Baer, E. Polymer 2006, 47, 2423.
6. Jacquelot, E.; Espuche, E.; Gerard, J. F.; Duchet, J.; Mazabraud, P. J Polym Sci Part B: Polym Phys 2006, 44, 431.
7. Charles, S.; Christopher, C.; Anastasios, L.; Douglas, H. J Membr Sci 2005, 263, 47.
8. Roberts, A. P.; Henry, B. M.; Sutton, A. P.; Grovenor, C. R. M.; Briggs, G. A. D.; Miyamoto, T.; Kano, M.; Tsukahara, Y.; Yanaka, M. J Membr Sci 2002, 208: 75.
9. Ke, Y. C.; Yang, Z. B.; Zhu, C. F. J Appl Polym Sci 2002, 85, 2677.
10. Ke, Y. C.; Long, C. F.; Qi, Z. N. J Appl Polym Sci 1999, 71, 1139.

11. Kim, S. W.; Jo, W. H.; Lee, M. S.; Ko, M. B.; Jho, J. Y. Polym J 2002, 34, 103.
12. Chang, J. H.; An, Y. U. J Polym Sci Part B: Polym Phys 2002, 40, 670.
13. Ke, Y. C.; Stroeve, P. Polymer-Layered Silicate and Silica Nanocomosite; Elsevier: Armstardam, 2006; p 5.
14. Xia, Y. F.M.D. Dissertation; China University of Petroleum: Beijing, 2008, 5 (Available at: http://libcd2.cup.edu.cn:8080). Accessed July 20, 2008.
15. Achilias, D. S.; Bikiaris, D. N.; Karavelidis, V.; Karayannidis, G. P. Eur Polym J 2008, 44, 3096.
16. Wu, T. B.; Ke, Y. C. Thin Solid Films 2007, 515, 5220.
17. Schurr, O. The Type and Distribution of Sites as Assessed by the Accessibility; Washington, D. C.; (Available at: http://pubs.acs.org/doi/full/10.1021/ma034130e). Accessed December 20, 2002.
18. Hirayama, Y.; Yoshinaga, T.; Kusuki, Y.; Ninomiyaa, K.; Sakakibarab, T.; Tamarib, T. J Membr Sci 1996, 111, 169.
19. Hirayama, Y.; Yoshinaga, T. J Membr Sci 1996, 111, 169.
20. Lan, T.; Psihongios, V.; Turner, S. R.; Connell, G. W.; Matayabas, J, James, C.; Gilmer, J. W. U.S. Pat.6376591 (2002).
21. Ke, Y. C.; Wu, T. B.; Xia, Y. F. Polymer 2007, 48, 3324.
22. Wu, T. B.; Ke, Y. C. Eur Polym J 2006, 42, 274.
23. Ke, Y. C.; Wu, T. B.; Yan, C. J.; Xu, C. M. China Particuol 2003, 1, 247.
24. Zhang, Y.; Zhang, J. M.; Lu, Y. L.; Duan, Y. X.; Yan, S. K.; Shen, D. Y. Macromolecules 2004, 37, 2532.
25. Wu, T. B.; Ke, Y. C. Polym Degrad Stab 2006, 91, 2205.
26. Wolf, C. J.; Boramann, J. A.; Grayson, M. A. J Polym Sci Phys Ed 1991, 29, 1533.
27. Wolf, C. J.; J Polym Sci Phys Ed 1992, 30, 113.
28. Wu, T. B. Ph.D. Dissertation; China University of Petroleum: Beijing, 2006, 5 (Available at: http://libcd2.cup.edu.cn: 8080). Accessed July 20, 2006.
29. Lee, S. W.; Ree, M.; Park, C. E.; Jung, Y. K.; Park, C. S.; Jin, Y. S.; Bae, D. C. Polymer 1999, 40: 7137.
30. Wang, R. Ph.D. Dissertation, Sichuan University: Sichaun, 2003, 5. (Available at: http://www.cnki.net/kcms/detail/detail.aspx?dbcode=CDFD&QueryID=0&CurRec=111&dbname=CDFD9908&filename=2003107324.nh&uid=WEEvREdiSUtucElBV1VGV2tYR0FyUDdUa201UUwrQTR3SnZZZDNhYURrVVNQYllDbkZuWUF5R2pXQld0NkFNPQ==). Accessed July 20, 2003.
31. Yuan, X. M.D. dissertation, Sichuan University, Sichuan, 2007.5. (Available at: http://dlib.edu.cnki.net/kns50/detail.aspx?QueryID=23&CurRec= 6). Accessed July 20, 2007.
32. Gao, X. F.; Jiang, L. Nature 2004, 432, 36.
33. Di, Q. F.; Shen, C.; Wang, Z. H.; Gu, C. Y.; Shi, L. Y.; Fang, H. P. Petrol Sci (Chin) 2009, 30, 125.